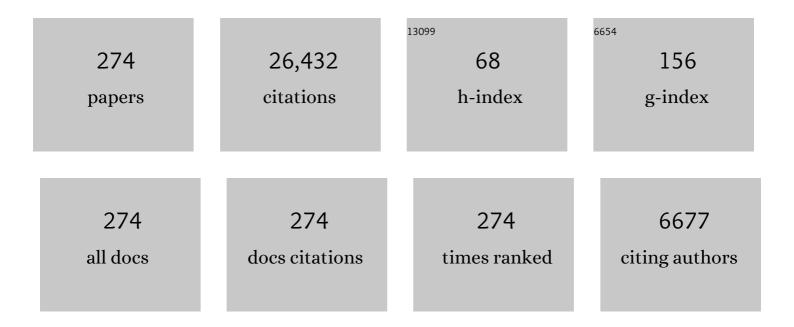
Yong-Sheng Liu

List of Publications by Year in descending order

Source: https://exaly.com/author-pdf/6864990/publications.pdf Version: 2024-02-01



#	Article	IF	CITATIONS
1	A new analytical mode and application of the laser ablation inductively coupled plasma mass spectrometer in the earth sciences. Science China Earth Sciences, 2022, 65, 182-196.	5.2	5
2	An Improved Procedure for the Determination of Trace Elements in Silicate Rocks Using NH ₄ HF ₂ Digestion. Geostandards and Geoanalytical Research, 2022, 46, 21-35.	3.1	4
3	Determination of carbon isotopes in carbonates (calcite, dolomite, magnesite, and siderite) by femtosecond laser ablation multi-collector ICP-MS. Journal of Analytical Atomic Spectrometry, 2022, 37, 278-288.	3.0	8
4	Formation of green-core clinopyroxene in continental basalts through magmatic differentiation and crustal assimilation: Insights from in-situ trace element and Pb isotopic compositions. Lithos, 2022, 410-411, 106587.	1.4	2
5	A new synthesis scheme of pyrite and chalcopyrite reference materials for <i>in situ</i> iron and sulfur isotope analysis using LA-MC-ICP-MS. Journal of Analytical Atomic Spectrometry, 2022, 37, 551-562.	3.0	16
6	Non-matrix-matched calibration of Mg isotopic ratios in silicate samples by fs-LA-MC-ICP-MS with low mass resolution under wet plasma conditions. Journal of Analytical Atomic Spectrometry, 2022, 37, 592-602.	3.0	10
7	Copper mobilization in the lower continental crust beneath cratonic margins, a Cu isotope perspective. Geochimica Et Cosmochimica Acta, 2022, 322, 43-57.	3.9	11
8	Origin of low-MgO primitive intraplate alkaline basalts from partial melting of carbonate-bearing eclogite sources. Geochimica Et Cosmochimica Acta, 2022, 324, 240-261.	3.9	13
9	Accurate Determination of Zr Isotopic Ratio in Zircons by Femtosecond Laser Ablation MC-ICP-MS with "Wet―Plasma Technique. Journal of Earth Science (Wuhan, China), 2022, 33, 67-75.	3.2	23
10	Decoupled Zn-Sr-Nd isotopic composition of continental intraplate basalts caused by two-stage melting process. Geochimica Et Cosmochimica Acta, 2022, 326, 234-252.	3.9	13
11	Isotopic Analysis by Laser Ablation Solution Sampling MC-ICP-MS─An Example of Boron. Analytical Chemistry, 2022, 94, 1286-1293.	6.5	5
12	Determination of the Isotopic Composition of Ytterbium by MC-ICP-MS Using an Optimized Regression Model. Analytical Chemistry, 2022, 94, 7200-7209.	6.5	1
13	High-precision magnesium isotope analysis of carbonates by laser ablation MC-ICP-MS using wet and dry conditions. Journal of Analytical Atomic Spectrometry, 2022, 37, 1665-1674.	3.0	4
14	Bulk compositions of the Chang'E-5 lunar soil: Insights into chemical homogeneity, exotic addition, and origin of landing site basalts. Geochimica Et Cosmochimica Acta, 2022, 335, 284-296.	3.9	38
15	Anoxia may delay biotic recovery from the Late Ordovician mass extinction. Science Bulletin, 2021, 66, 414-416.	9.0	3
16	Non-matrix-matched analysis of U-Th-Pb geochronology of bastnäte by laser ablation inductively coupled plasma mass spectrometry. Science China Earth Sciences, 2021, 64, 667-676.	5.2	8
17	Investigation of nitrogen addition, position effect and mismatch intensity effect in Li isotopic analysis by nanosecond laser ablation multi-collector inductively coupled plasma mass spectrometry. Spectrochimica Acta, Part B: Atomic Spectroscopy, 2021, 177, 106074.	2.9	7
18	Calcium Stable Isotopes of Tonga and Mariana Arc Lavas: Implications for Slab Fluidâ€Mediated Carbonate Transfer in Cold Subduction Zones. Journal of Geophysical Research: Solid Earth, 2021, 126, e2020JB020207.	3.4	4

#	Article	IF	CITATIONS
19	Transformation from oxidized to reduced alkaline magmas in the northern North China Craton. Lithos, 2021, 390-391, 106104.	1.4	2
20	Recycling of Paleo-Asian Ocean carbonates and its influence on the lithospheric composition of the North China Craton. Science China Earth Sciences, 2021, 64, 1346-1362.	5.2	5
21	Massive carbon storage in convergent margins initiated by subduction of limestone. Nature Communications, 2021, 12, 4463.	12.8	21
22	Mesoarchean continental intraplate volcanism and sedimentation: The case of the Simlipal basin, Singhbhum Craton, eastern India. Precambrian Research, 2021, 361, 106245.	2.7	12
23	Reconstruction of primary alkaline magma composition from mineral archives: Decipher mantle metasomatism by carbonated sediment. Chemical Geology, 2021, 577, 120279.	3.3	5
24	The largest negative carbon isotope excursions in Neoproterozoic carbonates caused by recycled carbonatite volcanic ash. Science Bulletin, 2021, 66, 1925-1931.	9.0	15
25	Integrated biochemostratigraphy of the Permian-Triassic boundary beds in a shallow carbonate platform setting (Yangou, South China). Clobal and Planetary Change, 2021, 206, 103583.	3.5	5
26	A high-performance method for direct determination of ultra-trace REEs in geological samples by ICP-MS using a designed heating-condensing system. Journal of Analytical Atomic Spectrometry, 2021, 36, 723-732.	3.0	5
27	Early Paleozoic Arc Magmatism and Accretionary Orogenesis in the Indochina Block, Southeast Asia. Journal of Geology, 2021, 129, 33-48.	1.4	7
28	Deciphering the origin of a basanite-alkali basalt-tholeiite suite using Zn isotopes. Chemical Geology, 2021, 585, 120585.	3.3	6
29	Tanz zircon megacrysts: a new zircon reference material for the microbeam determination of U–Pb ages and Zr–O isotopes. Journal of Analytical Atomic Spectrometry, 2021, 36, 2715-2734.	3.0	25
30	Heterogeneous potassium isotopic composition of the upper continental crust. Geochimica Et Cosmochimica Acta, 2020, 278, 122-136.	3.9	72
31	Improved in-situ Determination of Sr Isotope Ratio in Silicate Samples Using LA-MC-ICP-MS and Its Wider Application for Fused Rock Powder. Journal of Earth Science (Wuhan, China), 2020, 31, 262-270.	3.2	5
32	An SPO-induced CPO in composite mantle xenoliths correlated with increasing melt-rock interaction. Geochimica Et Cosmochimica Acta, 2020, 278, 199-218.	3.9	17
33	How mafic was the Archean upper continental crust? Insights from Cu and Ag in ancient glacial diamictites. Geochimica Et Cosmochimica Acta, 2020, 278, 16-29.	3.9	35
34	Calcium isotopic compositions of oceanic crust at various spreading rates. Geochimica Et Cosmochimica Acta, 2020, 278, 272-288.	3.9	37
35	Lower Triassic carbonate l´238U record demonstrates expanded oceanic anoxia during Smithian Thermal Maximum and improved ventilation during Smithian-Spathian boundary cooling event. Palaeogeography, Palaeoclimatology, Palaeoecology, 2020, 539, 109393.	2.3	21
36	Oxidization of the mantle caused by sediment recycling may contribute to the formation of iron-rich mantle melts. Science Bulletin, 2020, 65, 519-521.	9.0	10

#	Article	IF	CITATIONS
37	A simple single-stage extraction method for Mo separation from geological samples for isotopic analysis by MC-ICP-MS. Journal of Analytical Atomic Spectrometry, 2020, 35, 145-154.	3.0	12
38	Generation of continental intraplate alkali basalts and implications for deep carbon cycle. Earth-Science Reviews, 2020, 201, 103073.	9.1	30
39	Metasomatized lithospheric mantle for Mesozoic giant gold deposits in the North China craton. Geology, 2020, 48, 169-173.	4.4	85
40	Sulfide-bearing cumulates in deep continental arcs: The missing copper reservoir. Earth and Planetary Science Letters, 2020, 531, 115971.	4.4	57
41	Calcium isotope compositions of mantle pyroxenites. Geochimica Et Cosmochimica Acta, 2020, 270, 144-159.	3.9	24
42	Reply to Comment from Zafar, Leng and Chen on "Sulfide-bearing cumulates in deep continental arcs: The missing copper reservoir―by Chen et al. (Earth Planet. Sci. Lett. 531 (2020) 115971). Earth and Planetary Science Letters, 2020, 551, 116592.	4.4	0
43	Recycling of granulitic lower crust into the mantle. Lithos, 2020, 378-379, 105812.	1.4	2
44	Mantle degassing related to changing redox and thermal conditions during the Precambrian supercontinent cycle. Precambrian Research, 2020, 350, 105895.	2.7	6
45	Multiple metasomatism of the lithospheric mantle beneath the northeastern North China Craton. Lithos, 2020, 374-375, 105719.	1.4	4
46	The zirconium stable isotope compositions of 22 geological reference materials, 4 zircons and 3 standard solutions. Chemical Geology, 2020, 555, 119791.	3.3	27
47	Nonâ€Matrixâ€Matched Determination of Thâ€Pb Ages in Zircon, Monazite and Xenotime by Laser Ablationâ€Inductively Coupled Plasmaâ€Mass Spectrometry. Geostandards and Geoanalytical Research, 2020, 44, 653-668.	3.1	15
48	Compositional and pressure controls on calcium and magnesium isotope fractionation in magmatic systems. Geochimica Et Cosmochimica Acta, 2020, 290, 257-270.	3.9	22
49	Anomalous marine calcium cycle linked to carbonate factory change after the Smithian Thermal Maximum (Early Triassic). Earth-Science Reviews, 2020, 211, 103418.	9.1	13
50	Lithospheric modification by carbonatitic to alkaline melts and deep carbon cycle: Insights from peridotite xenoliths of eastern China. Lithos, 2020, 378-379, 105789.	1.4	0
51	Mechanism of Paleoarchean continental crust formation as archived in granitoids from the northern part of Singhbhum Craton, eastern India. Geological Society Special Publication, 2020, 489, 189-214.	1.3	13
52	A high performance method for the accurate and precise determination of silicon isotopic compositions in bulk silicate rock samples using laser ablation MC-ICP-MS. Journal of Analytical Atomic Spectrometry, 2020, 35, 1887-1896.	3.0	8
53	Determination of the Isotopic Composition of an Enriched Hafnium Spike by MCâ€ICPâ€MS Using a Regression Model. Geostandards and Geoanalytical Research, 2020, 44, 753-762.	3.1	1
54	Melting of a hydrous peridotite mantle source under the Emeishan large igneous province. Earth-Science Reviews, 2020, 207, 103253.	9.1	19

#	Article	IF	CITATIONS
55	Direct and rapid multi-element analysis of wine samples in their natural liquid state by laser ablation ICPMS. Journal of Analytical Atomic Spectrometry, 2020, 35, 1071-1079.	3.0	11
56	Archean, highly unradiogenic lead in shallow cratonic mantle. Geology, 2020, 48, 584-588.	4.4	3
57	lso-Compass: new freeware software for isotopic data reduction of LA-MC-ICP-MS. Journal of Analytical Atomic Spectrometry, 2020, 35, 1087-1096.	3.0	132
58	Mesoproterozoic paleo-redox changes during 1500–1400ÂMa in the Yanshan Basin, North China. Precambrian Research, 2020, 347, 105835.	2.7	12
59	Zinc isotopic composition of the lower continental crust estimated from lower crustal xenoliths and granulite terrains. Geochimica Et Cosmochimica Acta, 2020, 276, 92-108.	3.9	12
60	High-precision stable zirconium isotope ratio measurements by double spike thermal ionization mass spectrometry. Journal of Analytical Atomic Spectrometry, 2020, 35, 736-745.	3.0	32
61	The effect of host magma infiltration on the Pb isotopic systematics of lower crustal xenolith: An in-situ study from Hannuoba, North China. Lithos, 2020, 366-367, 105556.	1.4	4
62	Rutile records for the cooling history of the Trans-North China orogen from assembly to break-up of the Columbia supercontinent. Precambrian Research, 2020, 346, 105763.	2.7	10
63	Comparative Determination of Mass Fractions of Elements with Variable Chalcophile Affinities in Geological Reference Materials with and without HFâ€desilicification. Geostandards and Geoanalytical Research, 2020, 44, 501-521.	3.1	16
64	Lithium isotope compositions of the Yangtze River headwaters: Weathering in high-relief catchments. Geochimica Et Cosmochimica Acta, 2020, 280, 46-65.	3.9	47
65	Platinum group element mobilization in the mantle enhanced by recycled sedimentary carbonate. Earth and Planetary Science Letters, 2020, 541, 116262.	4.4	15
66	Performance Evaluation of Atmospheric Pressure Glow Discharge-Optical Emission Spectrometry for the Determination of Sodium, Lithium, Calcium and Magnesium Using Membrane Desolvation. Atomic Spectroscopy, 2020, 41, 57-63.	1.2	9
67	An Effective Oxide Interference Correction on Sc and REE for Routine Analyses of Geological Samples by Inductively Coupled Plasma-Mass Spectrometry. Journal of Earth Science (Wuhan, China), 2019, 30, 1302-1310.	3.2	12
68	Determination of Zr isotopic ratios in zircons using laser-ablation multiple-collector inductively coupled-plasma mass-spectrometry. Journal of Analytical Atomic Spectrometry, 2019, 34, 1800-1809.	3.0	43
69	Deep carbon cycle in subduction zones. Science China Earth Sciences, 2019, 62, 1764-1782.	5.2	23
70	Determination of Gallium Isotopic Compositions in Reference Materials. Geostandards and Geoanalytical Research, 2019, 43, 701-714.	3.1	13
71	Building the core of a Paleoarchean continent: Evidence from granitoids of Singhbhum Craton, eastern India. Precambrian Research, 2019, 335, 105436.	2.7	34
72	Calcium isotope fractionation during magmatic processes in the upper mantle. Geochimica Et Cosmochimica Acta, 2019, 249, 121-137.	3.9	58

Yong-Sheng Liu

#	Article	IF	CITATIONS
73	The Role of Earth's Deep Volatile Cycling in the Generation of Intracontinental Highâ€Mg Andesites: Implication for Lithospheric Thinning Beneath the North China Craton. Journal of Geophysical Research: Solid Earth, 2019, 124, 1305-1323.	3.4	16
74	Lithospheric transformation of the northern North China Craton by changing subduction style of the Paleo-Asian oceanic plate: Constraints from peridotite and pyroxenite xenoliths in the Yangyuan basalts. Lithos, 2019, 328-329, 58-68.	1.4	15
75	Determination of Cl, Br, and I in Geological Materials by Sector Field Inductively Coupled Plasma Mass Spectrometry. Analytical Chemistry, 2019, 91, 8109-8114.	6.5	13
76	An improved in situ technique for the analysis of the Os isotope ratio in sulfides using laser ablation-multiple ion counter inductively coupled plasma mass spectrometry. Journal of Analytical Atomic Spectrometry, 2019, 34, 1546-1552.	3.0	4
77	U–Pb geochronology of wolframite by laser ablation inductively coupled plasma mass spectrometry. Journal of Analytical Atomic Spectrometry, 2019, 34, 1439-1446.	3.0	34
78	In situ calcium isotopic ratio determination in calcium carbonate materials and calcium phosphate materials using laser ablation-multiple collector-inductively coupled plasma mass spectrometry. Chemical Geology, 2019, 522, 16-25.	3.3	11
79	Accurate analysis of Li isotopes in tourmalines by LA-MC-ICP-MS under "wet―conditions with non-matrix-matched calibration. Journal of Analytical Atomic Spectrometry, 2019, 34, 1145-1153.	3.0	22
80	Determination of major and trace elements in geological samples by laser ablation solution sampling-inductively coupled plasma mass spectrometry. Journal of Analytical Atomic Spectrometry, 2019, 34, 1126-1134.	3.0	16
81	Implication of Mesoproterozoic (â^¼1.4†Ga) magmatism within microcontinents along the southern Central Asian Orogenic Belt. Precambrian Research, 2019, 327, 314-326.	2.7	38
82	Thermal-chemical conditions of the North China Mesozoic lithospheric mantle and implication for the lithospheric thinning of cratons. Earth and Planetary Science Letters, 2019, 516, 1-11.	4.4	42
83	Accurate Measurement of Lithium Isotopes in Eleven Carbonate Reference Materials by <scp>MC</scp> â€ <scp>ICP</scp> â€ <scp>MS</scp> with Soft Extraction Mode and 10 ¹² Ω Resistor Highâ€Gain Faraday Amplifiers. Geostandards and Geoanalytical Research, 2019, 43, 277-289.	3.1	22
84	Early Crustal Evolution as Recorded in the Granitoids of the Singhbhum and Western Dharwar Cratons. , 2019, , 741-792.		25
85	High-precision CopperandZinc Isotopic Measurements in Igneous RockStandards UsingLarge-geometry MC-ICP-MS. Atomic Spectroscopy, 2019, 40, 206-214.	1.2	20
86	场幔橄榄岩ä,碳é…,盢†"体äº∰»£ä½œç"ªåŠå…¶é‰′定特徕 Diqiu Kexue - Zhongguo Dizhi Da Geosciences, 2019, 44, 1113.	xue Xueba	o/Eąrth Scienc
87	Carbonate metasomatism in the lithospheric mantle: Implications for cratonic destruction in North China. Science China Earth Sciences, 2018, 61, 711-729.	5.2	49
88	A Rapid Acid Digestion Technique for the Simultaneous Determination of Bromine and Iodine in Fiftyâ€Three Chinese Soils and Sediments by <scp>ICP</scp> â€ <scp>MS</scp> . Geostandards and Geoanalytical Research, 2018, 42, 309-318.	3.1	18
89	Determination of Smâ€Nd Isotopic Compositions in Fifteen Geological Materials Using Laser Ablation MCâ€ICPâ€MS and Application to Monazite Geochronology of Metasedimentary Rock in the North China Craton. Geostandards and Geoanalytical Research, 2018, 42, 379-394.	3.1	16
90	Early Neoarchaean A-type granitic magmatism by crustal reworking in Singhbhum craton: Evidence from Pala Lahara area, Orissa. Journal of Earth System Science, 2018, 127, 1.	1.3	29

#	Article	IF	CITATIONS
91	Improved in situ Sr isotopic analysis by a 257 nm femtosecond laser in combination with the addition of nitrogen for geological minerals. Chemical Geology, 2018, 479, 10-21.	3.3	70
92	Geochemical evidence for Paleozoic crustal growth and tectonic conversion in the Northern Beishan Orogenic Belt, southern Central Asian Orogenic Belt. Lithos, 2018, 302-303, 189-202.	1.4	30
93	Constant Cu/Ag in upper mantle and oceanic crust: Implications for the role of cumulates during the formation of continental crust. Earth and Planetary Science Letters, 2018, 493, 25-35.	4.4	24
94	Elemental fractionation and quantification of geological standard samples by nanosecond-laser ablation. Spectrochimica Acta, Part B: Atomic Spectroscopy, 2018, 143, 55-62.	2.9	9
95	Development of sulfide reference materials for <i>in situ</i> platinum group elements and S–Pb isotope analyses by LA-(MC)-ICP-MS. Journal of Analytical Atomic Spectrometry, 2018, 33, 2172-2183.	3.0	24
96	Subducted Mg-rich carbonates into the deep mantle wedge. Earth and Planetary Science Letters, 2018, 503, 118-130.	4.4	39
97	Step-like growth of the continental crust in South China: evidence from detrital zircons in Yangtze River sediments. Lithos, 2018, 320-321, 155-171.	1.4	10
98	Reassessment of the influence of carrier gases He and Ar on signal intensities in 193Ânm excimer LA-ICP-MS analysis. Journal of Analytical Atomic Spectrometry, 2018, 33, 1655-1663.	3.0	31
99	Calcium isotope evidence for subduction-enriched lithospheric mantle under the northern North China Craton. Geochimica Et Cosmochimica Acta, 2018, 238, 55-67.	3.9	39
100	Water Vapor-Assisted "Universal―Nonmatrix-Matched Analytical Method for the in Situ U–Pb Dating of Zircon, Monazite, Titanite, and Xenotime by Laser Ablation-Inductively Coupled Plasma Mass Spectrometry. Analytical Chemistry, 2018, 90, 9016-9024.	6.5	61
101	Radiogenic Pb reservoir contributes to the rare earth element (REE) enrichment in South Qinling carbonatites. Chemical Geology, 2018, 494, 80-95.	3.3	32
102	Magma Recharge and Reactive Bulk Assimilation in Enclave-Bearing Granitoids, Tonglu, South China. Journal of Petrology, 2018, 59, 795-824.	2.8	12
103	High-precision Ca isotopic measurement using a large geometry high resolution MC-ICP-MS with a dummy bucket. Journal of Analytical Atomic Spectrometry, 2018, 33, 1707-1719.	3.0	34
104	Olivine Oxygen Isotope Evidence for Intracontinental Recycling of Delaminated Continental Crust. Geochemistry, Geophysics, Geosystems, 2018, 19, 1913-1924.	2.5	13
105	Subduction of Indian continent beneath southern Tibet in the latest Eocene (~ 35 Ma): Insights from the Quguosha gabbros in southern Lhasa block. Gondwana Research, 2017, 41, 77-92.	6.0	49
106	A precise zircon Th-Pb age of carbonatite sills from the world's largest Bayan Obo deposit: Implications for timing and genesis of REE-Nb mineralization. Precambrian Research, 2017, 291, 202-219.	2.7	57
107	Low-δ13C carbonates in the Miocene basalt of the northern margin of the North China Craton: Implications for deep carbon recycling. Journal of Asian Earth Sciences, 2017, 144, 110-125.	2.3	7
108	Improved in situ Li isotopic ratio analysis of silicates by optimizing signal intensity, isotopic ratio stability and intensity matching using ns-LA-MC-ICP-MS. Journal of Analytical Atomic Spectrometry, 2017, 32, 834-842.	3.0	19

#	Article	IF	CITATIONS
109	SiC-dominated ultra-reduced mineral assemblage in carbonatitic xenoliths from the Dalihu basalt, Inner Mongolia, China. American Mineralogist, 2017, 102, 312-320.	1.9	8
110	Re–Os isotope evidence from Mesozoic and Cenozoic basalts for secular evolution of the mantle beneath the North China Craton. Contributions To Mineralogy and Petrology, 2017, 172, 1.	3.1	18
111	Calcium Isotopic Compositions of Sixteen <scp>USCS</scp> Reference Materials. Geostandards and Geoanalytical Research, 2017, 41, 93-106.	3.1	55
112	Generation and evolution of Palaeoarchaean continental crust in the central part of the Singhbhum craton, eastern India. Precambrian Research, 2017, 298, 268-291.	2.7	106
113	The assembly of Rodinia: The correlation of early Neoproterozoic (ca. 900 Ma) high-grade metamorphism and continental arc formation in the southern Beishan Orogen, southern Central Asian Orogenic Belt (CAOB). Precambrian Research, 2017, 290, 32-48.	2.7	453
114	Crust recycling induced compositional-temporal-spatial variations of Cenozoic basalts in the Trans-North China Orogen. Lithos, 2017, 274-275, 383-396.	1.4	31
115	Deep carbon cycles constrained by a large-scale mantle Mg isotope anomaly in eastern China. National Science Review, 2017, 4, 111-120.	9.5	240
116	The 131–134 Ma A-type granites from northern Zhejiang Province, South China: Implications for partial melting of the Neoproterozoic lower crust. Lithos, 2017, 294-295, 39-52.	1.4	15
117	Accurate determination of sulfur isotopes (<i>δ</i> ³³ S and <i>δ</i> ³⁴ S) in sulfides and elemental sulfur by femtosecond laser ablation MC-ICP-MS with non-matrix matched calibration. Journal of Analytical Atomic Spectrometry, 2017, 32, 2341-2351.	3.0	25
118	87Sr/86Sr evidence from the epeiric Martin Ridge Basin for enhanced carbonate weathering during the Hirnantian. Scientific Reports, 2017, 7, 11348.	3.3	8
119	Comparison of signal intensities and elemental fractionation in 257 nm femtosecond LA-ICP-MS using He and Ar as carrier gases. Journal of Analytical Atomic Spectrometry, 2017, 32, 2217-2225.	3.0	12
120	Carbonated sediment recycling and its contribution to lithospheric refertilization under the northern North China Craton. Chemical Geology, 2017, 466, 641-653.	3.3	41
121	In-situ trace element and Sr isotopic compositions of mantle xenoliths constrain two-stage metasomatism beneath the northern North China Craton. Lithos, 2017, 288-289, 338-351.	1.4	31
122	Quantitative analysis of major and trace elements in NH4HF2-modified silicate rock powders by laser ablation - inductively coupled plasma mass spectrometry. Analytica Chimica Acta, 2017, 983, 149-159.	5.4	12
123	Phosphorus zoning as a recorder of crystal growth kinetics: application to second-generation olivine in mantle xenoliths from the Cima Volcanic Field. Contributions To Mineralogy and Petrology, 2017, 172, 1.	3.1	9
124	Pressure-dependent compatibility of iron in garnet: Insights into the origin of ferropicritic melt. Geochimica Et Cosmochimica Acta, 2017, 197, 356-377.	3.9	28
125	Widespread Neoarchean (~ 2.7–2.6 Ga) magmatism of the Yangtze craton, South China, as revealed by modern river detrital zircons. Gondwana Research, 2017, 42, 1-12.	6.0	36
126	Trace element and <scp>S</scp> r isotope records of multiâ€episode carbonatite metasomatism on the eastern margin of the <scp>N</scp> orth <scp>C</scp> hina <scp>C</scp> raton. Geochemistry, Geophysics, Geosystems, 2017, 18, 220-237.	2.5	35

#	Article	IF	CITATIONS
127	Paleo-Asian Oceanic slab under the North China Craton revealed by carbonatites derived from subducted limestones: REPLY. Geology, 2017, 45, e414-e414.	4.4	Ο
128	Ablation Characteristic of Ilmenite using <scp>UV</scp> Nanosecond and Femtosecond Lasers: Implications for Nonâ€Matrixâ€Matched Quantification. Geostandards and Geoanalytical Research, 2016, 40, 477-491.	3.1	11
129	High precision measurements of gallium isotopic compositions in geological materials by MC-ICP-MS. Journal of Analytical Atomic Spectrometry, 2016, 31, 1673-1679.	3.0	21
130	In situ measurement of Os isotopic ratios in sulfides calibrated against ultra-fine particle standards using LA-MC-ICP-MS. Journal of Analytical Atomic Spectrometry, 2016, 31, 1414-1422.	3.0	13
131	Green and Fast Laser Fusion Technique for Bulk Silicate Rock Analysis by Laser Ablation-Inductively Coupled Plasma Mass Spectrometry. Analytical Chemistry, 2016, 88, 10088-10094.	6.5	18
132	Accurate Determination of Sr Isotopic Compositions in Clinopyroxene and Silicate Glasses by <scp>LA</scp> â€ <scp>MC</scp> â€ <scp>ICP</scp> â€ <scp>MS</scp> . Geostandards and Geoanalytical Research, 2016, 40, 85-99.	3.1	100
133	An Investigation of Digestion Methods for Trace Elements in Bauxite and Their Determination in Ten Bauxite Reference Materials Using Inductively Coupled Plasmaâ€Mass Spectrometry. Geostandards and Geoanalytical Research, 2016, 40, 195-216.	3.1	21
134	Formation of the Giant Bayan Obo Deposit by ca. 1.3 Ga Carbonatitic Magmatism and its Link with Continental Rifting in the Columbia Supercontinent. Acta Geologica Sinica, 2016, 90, 195-196.	1.4	1
135	Al-in-olivine thermometry evidence for the mantle plume origin of the Emeishan large igneous province. Lithos, 2016, 266-267, 362-366.	1.4	25
136	Paleo-Asian oceanic slab under the North China craton revealed by carbonatites derived from subducted limestones. Geology, 2016, 44, 1039-1042.	4.4	67
137	Direct lead isotope analysis in Hg-rich sulfides by LA-MC-ICP-MS with a gas exchange device and matrix-matched calibration. Analytica Chimica Acta, 2016, 948, 9-18.	5.4	48
138	Calibration and correction of LA-ICP-MS and LA-MC-ICP-MS analyses for element contents and isotopic ratios. Solid Earth Sciences, 2016, 1, 5-27.	1.7	238
139	In situ sulfur isotopes (δ34 S and δ33 S) analyses in sulfides and elemental sulfur using high sensitivity cones combined with the addition of nitrogen by laser ablation MC-ICP-MS. Analytica Chimica Acta, 2016, 911, 14-26.	5.4	126
140	Magnesium isotopic composition of the deep continental crust. American Mineralogist, 2016, 101, 243-252.	1.9	42
141	Paleo-Asian oceanic subduction-related modification of the lithospheric mantle under the North China Craton: Evidence from peridotite xenoliths in the Datong basalts. Lithos, 2016, 261, 109-127.	1.4	27
142	Accurate determination of lithium isotope ratios by MC-ICP-MS without strict matrix-matching by using a novel washing method. Journal of Analytical Atomic Spectrometry, 2016, 31, 390-397.	3.0	63
143	First direct evidence of sedimentary carbonate recycling in subduction-related xenoliths. Scientific Reports, 2015, 5, 11547.	3.3	57
144	In situ Nd isotope analyses in geological materials with signal enhancement and non-linear mass dependent fractionation reduction using laser ablation MC-ICP-MS. Journal of Analytical Atomic Spectrometry, 2015, 30, 232-244.	3.0	69

#	Article	IF	CITATIONS
145	Improved performance of a shielded torch using ethanol in inductively coupled plasma–sector field mass spectrometry. Spectrochimica Acta, Part B: Atomic Spectroscopy, 2015, 106, 36-44.	2.9	12
146	Accurate determination of elements in silicate glass by nanosecond and femtosecond laser ablation ICP-MS at high spatial resolution. Chemical Geology, 2015, 400, 11-23.	3.3	32
147	Overlapping Sr–Nd–Hf–O isotopic compositions in Permian mafic enclaves and host granitoids in Alxa Block, NW China: Evidence for crust–mantle interaction and implications for the generation of silicic igneous provinces. Lithos, 2015, 230, 133-145.	1.4	49
148	Geochemical and geochronological evidence for a former early Neoproterozoic microcontinent in the South Beishan Orogenic Belt, southernmost Central Asian Orogenic Belt. Precambrian Research, 2015, 266, 409-424.	2.7	64
149	Further investigation into ICP-induced elemental fractionation in LA-ICP-MS using a local aerosol extraction strategy. Journal of Analytical Atomic Spectrometry, 2015, 30, 941-949.	3.0	19
150	Improved Interâ€calibration of Faraday Cup and Ion Counting for <i>In Situ</i> Pb Isotope Measurements Using LAâ€MCâ€ICPâ€MS: Application to the Study of the Origin of the Fangshan Pluton, North China. Geostandards and Geoanalytical Research, 2015, 39, 467-487.	3.1	27
151	In-situ U-Pb dating of uraninite by fs-LA-ICP-MS. Science China Earth Sciences, 2015, 58, 1731-1740.	5.2	38
152	Episodic Paleoarchean-Paleoproterozoic (3.3–2.0 Ga) granitoid magmatism in Yangtze Craton, South China: Implications for late Archean tectonics. Precambrian Research, 2015, 270, 246-266.	2.7	125
153	Accuracy of LA-ICPMS zircon U-Pb age determination: An inter-laboratory comparison. Science China Earth Sciences, 2015, 58, 1722-1730.	5.2	80
154	Review of High-Precision Sr Isotope Analyses of Low-Sr Geological Samples. Journal of Earth Science (Wuhan, China), 2015, 26, 763-774.	3.2	21
155	Refertilization-driven destabilization of subcontinental mantle and the importance of initial lithospheric thickness for the fate of continents. Earth and Planetary Science Letters, 2015, 409, 225-231.	4.4	58
156	"Wave―Signal-Smoothing and Mercury-Removing Device for Laser Ablation Quadrupole and Multiple Collector ICPMS Analysis: Application to Lead Isotope Analysis. Analytical Chemistry, 2015, 87, 1152-1157.	6.5	415
157	Mesozoic–Cenozoic mantle evolution beneath the North China Craton: A new perspective from Hf–Nd isotopes of basalts. Gondwana Research, 2015, 27, 1574-1585.	6.0	54
158	Neoarchaean crustal growth by combined arc–plume action: evidence from the Kadiri Greenstone Belt, eastern Dharwar craton, India. Geological Society Special Publication, 2015, 389, 135-163.	1.3	20
159	Silicate melt inclusions in clinopyroxene phenocrysts from mafic dikes in the eastern North China Craton: Constraints on melt evolution. Journal of Asian Earth Sciences, 2015, 97, 150-168.	2.3	8
160	Methane-bearing melt inclusion in olivine phenocryst in Cenozoic alkaline basalt from Eastern China and its geological significance. Chinese Science Bulletin, 2015, 60, 1310-1319.	0.7	4
161	Late Cretaceous magmatism in Mamba area, central Lhasa subterrane: Products of back-arc extension of Neo-Tethyan Ocean?. Gondwana Research, 2014, 26, 505-520.	6.0	51
162	Episodic Mesozoic thickening and reworking of the North China Archean lower crust correlated to the fast-spreading Pacific plate. Journal of Asian Earth Sciences, 2014, 80, 63-74.	2.3	7

#	Article	IF	CITATIONS
163	Thermal-tectonic history of the Baogutu porphyry Cu deposit, West Junggar as constrained from zircon U–Pb, biotite Ar/Ar and zircon/apatite (U–Th)/He dating. Journal of Asian Earth Sciences, 2014, 79, 741-758.	2.3	50
164	3.45 Ga granitic gneisses from the Yangtze Craton, South China: Implications for Early Archean crustal growth. Precambrian Research, 2014, 242, 82-95.	2.7	245
165	Origin and evolution of granitoids associated with the Kadiri greenstone belt, eastern Dharwar craton: A history of orogenic to anorogenic magmatism. Precambrian Research, 2014, 246, 64-90.	2.7	60
166	Signal enhancement in laser ablation inductively coupled plasma-mass spectrometry using water and/or ethanol vapor in combination with a shielded torch. Journal of Analytical Atomic Spectrometry, 2014, 29, 536.	3.0	26
167	Determination of boron isotope compositions of geological materials by laser ablation MC-ICP-MS using newly designed high sensitivity skimmer and sample cones. Chemical Geology, 2014, 386, 22-30.	3.3	39
168	Titanite evidence for Triassic thickened lower crust along southeastern margin of North China Craton. Lithos, 2014, 206-207, 277-288.	1.4	9
169	Collision-related genesis of the Sharang porphyry molybdenum deposit, Tibet: Evidence from zircon U–Pb ages, Re–Os ages and Lu–Hf isotopes. Ore Geology Reviews, 2014, 56, 312-326.	2.7	79
170	Depositional environment and tectonic implications of the Paleoproterozoic BIF in Changyi area, eastern North China Craton: Evidence from geochronology and geochemistry of the metamorphic wallrocks. Ore Geology Reviews, 2014, 61, 52-72.	2.7	14
171	U–Pb zircon chronology, geochemistry and isotopes of the Changyi banded iron formation in the eastern Shandong Province: Constraints on BIF genesis and implications for Paleoproterozoic tectonic evolution of the North China Craton. Ore Geology Reviews, 2014, 56, 472-486.	2.7	47
172	Linking continental deep subduction with destruction of a cratonic margin: strongly reworked North China SCLM intruded in the Triassic Sulu UHP belt. Contributions To Mineralogy and Petrology, 2014, 168, 1.	3.1	103
173	Reprint of "Depositional environment and tectonic implications of the Paleoproterozoic BIF in Changyi area, eastern North China Craton: Evidence from geochronology and geochemistry of the metamorphic wallrocks― Ore Geology Reviews, 2014, 63, 444-464.	2.7	5
174	Pyroxenite and peridotite xenoliths from Hexigten, Inner Mongolia: Insights into the Paleo-Asian Ocean subduction-related melt/fluid–peridotite interaction. Geochimica Et Cosmochimica Acta, 2014, 140, 435-454.	3.9	40
175	LA - I CP -MS微区原ä½å‡†ç¡®å^†æžå«æ°´ç¡éç›çŸ¿ç‰©ä¸»é‡å'Œå¾®é‡åƒç´. Diqiu Kexue - Zhongguo Geosciences, 2014, 33, 525.	o Dizhi Da 0.5	xue Xuebao 1
176	Applications of LA-ICP-MS in the elemental analyses of geological samples. Science Bulletin, 2013, 58, 3863-3878.	1.7	81
177	Magma source and tectonics of the Xiangshanzhong mafic–ultramafic intrusion in the Central Asian Orogenic Belt, NW China, traced from geochemical and isotopic signatures. Lithos, 2013, 170-171, 144-163.	1.4	39
178	The generation and evolution of Archean continental crust in the Dunhuang block, northeastern Tarim craton, northwestern China. Precambrian Research, 2013, 235, 251-263.	2.7	117
179	Rapid bulk rock decomposition by ammonium fluoride (NH4F) in open vessels at an elevated digestion temperature. Chemical Geology, 2013, 355, 144-152.	3.3	41
180	In-situ trace elements and Li and Sr isotopes in peridotite xenoliths from Kuandian, North China Craton: Insights into Pacific slab subduction-related mantle modification. Chemical Geology, 2013, 354, 107-123.	3.3	62

#	Article	IF	CITATIONS
181	Rare-earth element patterns in conodont albid crowns: Evidence for massive inputs of volcanic ash during the latest Permian biocrisis?. Global and Planetary Change, 2013, 105, 135-151.	3.5	107
182	Multiple exsolutions in a rare clinopyroxene megacryst from the Hannuoba basalt, North China: Implications for subducted slab-related crustal thickening and recycling. Lithos, 2013, 177, 136-147.	1.4	16
183	Evolution of the lithospheric mantle beneath the southeastern North China Craton: Constraints from mafic dikes in the Jiaobei terrain. Gondwana Research, 2013, 24, 601-621.	6.0	118
184	Crust–mantle interaction beneath the Luxi Block, eastern North China Craton: Evidence from coexisting mantle- and crust-derived enclaves in a quartz monzonite pluton. Lithos, 2013, 177, 1-16.	1.4	31
185	Simultaneous Determination of Major and Trace Elements in Fused Volcanic Rock Powders Using a Hermetic Vessel Heater and <scp>LA</scp> â€ <scp>ICP</scp> â€ <scp>MS</scp> . Geostandards and Geoanalytical Research, 2013, 37, 207-229.	3.1	31
186	Origin of the Yinshan epithermal-porphyry Cu–Au–Pb–Zn–Ag deposit, southeastern China: insights from geochemistry, Sr–Nd and zircon U–Pb–Hf–O isotopes. International Geology Review, 2013, 55, 1835-1864.	2.1	9
187	UPb zircon age and geochemical constraints on tectonic evolution of the Paleozoic accretionary orogenic system in the Tongbai orogen, central China. Tectonophysics, 2013, 599, 67-88.	2.2	104
188	2.6–2.7 Ga crustal growth in Yangtze craton, South China. Precambrian Research, 2013, 224, 472-490.	2.7	162
189	Crustal Melting and Flow beneath Northern Tibet: Evidence from Mid-Miocene to Quaternary Strongly Peraluminous Rhyolites in the Southern Kunlun Range. Journal of Petrology, 2012, 53, 2523-2566.	2.8	83
190	Reassessment of HF/HNO3 Decomposition Capability in the High-Pressure Digestion of Felsic Rocks for Multi-Element Determination by ICP-MS. Geostandards and Geoanalytical Research, 2012, 36, 271-289.	3.1	41
191	Cambrian bimodal volcanism in the Lhasa Terrane, southern Tibet: Record of an early Paleozoic Andean-type magmatic arc in the Australian proto-Tethyan margin. Chemical Geology, 2012, 328, 290-308.	3.3	288
192	Triassic high-Mg adakitic andesites from Linxi, Inner Mongolia: Insights into the fate of the Paleo-Asian ocean crust and fossil slab-derived melt–peridotite interaction. Chemical Geology, 2012, 328, 89-108.	3.3	79
193	U–Pb geochronology and geochemistry of the bedrocks and moraine sediments from the Windmill Islands: Implications for Proterozoic evolution of East Antarctica. Precambrian Research, 2012, 206-207, 52-71.	2.7	33
194	Early Palaeozoic highâ€pressure granulites from the Dunhuang block, northeastern Tarim Craton: constraints on continental collision in the southern Central Asian Orogenic Belt. Journal of Metamorphic Geology, 2012, 30, 753-768.	3.4	78
195	Improved in situ Hf isotope ratio analysis of zircon using newly designed X skimmer cone and jet sample cone in combination with the addition of nitrogen by laser ablation multiple collector ICP-MS. Journal of Analytical Atomic Spectrometry, 2012, 27, 1391.	3.0	857
196	An evolving magma chamber within extending lithosphere: An integrated geochemical, isotopic and zircon U–Pb geochronological study of the Gushan granite, eastern North China Craton. Journal of Asian Earth Sciences, 2012, 50, 27-43.	2.3	52
197	A "wire―signal smoothing device for laser ablation inductively coupled plasma mass spectrometry analysis. Spectrochimica Acta, Part B: Atomic Spectroscopy, 2012, 78, 50-57.	2.9	205
198	Remelting of Neoproterozoic relict volcanic arcs in the Middle Jurassic: Implication for the formation of the Dexing porphyry copper deposit, Southeastern China. Lithos, 2012, 150, 85-100.	1.4	78

#	Article	IF	CITATIONS
199	Total Rock Dissolution Using Ammonium Bifluoride (NH ₄ HF ₂) in Screw-Top Teflon Vials: A New Development in Open-Vessel Digestion. Analytical Chemistry, 2012, 84, 10686-10693.	6.5	77
200	Major and Trace Element Characteristics of Apatites in Granitoids from Central Kazakhstan: Implications for Petrogenesis and Mineralization. Resource Geology, 2012, 62, 63-83.	0.8	155
201	Crustal thickening prior to 38 Ma in southern Tibet: Evidence from lower crust-derived adakitic magmatism in the Gangdese Batholith. Gondwana Research, 2012, 21, 88-99.	6.0	225
202	Geochemistry, zircon U–Pb age and Hf isotope compositions of Paleoproterozoic aluminous A-type granites from the Kongling terrain, Yangtze Block: Constraints on petrogenesis and geologic implications. Gondwana Research, 2012, 22, 140-151.	6.0	169
203	Reassessment of HF/HNO ₃ Decomposition Capability in the High-Pressure Digestion of Felsic Rocks for Multi-Element Determination by ICP-MS. Geostandards and Geoanalytical Research, 2012, , no-no.	3.1	31
204	Early Jurassic high-K calc-alkaline and shoshonitic rocks from the Tongshi intrusive complex, eastern North China Craton: Implication for crust–mantle interaction and post-collisional magmatism. Lithos, 2012, 140-141, 183-199.	1.4	67
205	Reactivation of the Archean lower crust: Implications for zircon geochronology, elemental and Sr–Nd–Hf isotopic geochemistry of late Mesozoic granitoids from northwestern Jiaodong Terrane, the North China Craton. Lithos, 2012, 146-147, 112-127.	1.4	240
206	Contrasting matrix induced elemental fractionation in NIST SRM and rock glasses during laser ablation ICP-MS analysis at high spatial resolution. Journal of Analytical Atomic Spectrometry, 2011, 26, 425-430.	3.0	123
207	Accurate determinations of fifty-four major and trace elements in carbonate by LA–ICP-MS using normalization strategy of bulk components as 100%. Chemical Geology, 2011, 284, 283-295.	3.3	138
208	Geochemistry and Sr–Nd–Pb–Hf isotopes of the Mesozoic Dadian alkaline intrusive complex in the Sulu orogenic belt, eastern China: Implications for crust–mantle interaction. Chemical Geology, 2011, 285, 97-114.	3.3	38
209	Garnet–spinel–corundum–quartz-bearing titanohematite veins in eclogite from the Sulu ultrahigh-pressure terrane: Imprint of a short-lived, high-temperature metamorphic stage. Journal of Asian Earth Sciences, 2011, 42, 704-714.	2.3	5
210	Zircon U-Pb and Hf evidence for coupled subduction of oceanic and continental crust during the Carboniferous in the Huwan shear zone, western Dabie orogen, central China. Journal of Metamorphic Geology, 2011, 29, 233-249.	3.4	31
211	Direct Quantitative Determination of Trace Elements in Fineâ€Grained Whole Rocks by Laser Ablationâ€Inductively Coupled Plasmaâ€Mass Spectrometry. Geostandards and Geoanalytical Research, 2011, 35, 7-22.	3.1	10
212	Preliminary Characterisation of New Reference Materials for Microanalysis: Chinese Geological Standard Glasses CGSG-1, CGSG-2, CGSG-4 and CGSG-5. Geostandards and Geoanalytical Research, 2011, 35, 235-251.	3.1	55
213	Multiple crust–mantle interactions for the destruction of the North China Craton: Geochemical and Sr–Nd–Pb–Hf isotopic evidence from the Longbaoshan alkaline complex. Lithos, 2011, 122, 87-106.	1.4	64
214	Garnet-rich granulite xenoliths from the Hannuoba basalts, North China: Petrogenesis and implications for the Mesozoic crust-mantle interaction. Journal of Earth Science (Wuhan, China), 2010, 21, 669-691.	3.2	31
215	Reappraisement and refinement of zircon U-Pb isotope and trace element analyses by LA-ICP-MS. Science Bulletin, 2010, 55, 1535-1546.	1.7	1,347
216	Microgeochemistry of rutile and zircon in eclogites from the CCSD main hole: Implications for the fluid activity and thermo-history of the UHP metamorphism. Lithos, 2010, 115, 51-64.	1.4	26

#	Article	IF	CITATIONS
217	Melting-induced fluid flow during exhumation of gneisses of the Sulu ultrahigh-pressure terrane. Lithos, 2010, 120, 490-510.	1.4	85
218	Early Paleozoic (ca. 465 Ma) eclogites from Beishan (NW China) and their bearing on the tectonic evolution of the southern Central Asian Orogenic Belt. Journal of Asian Earth Sciences, 2010, 42, 715-715.	2.3	19
219	In situ U–Pb dating and trace element analysis of zircons in thin sections of eclogite: Refining constraints on the ultra high-pressure metamorphism of the Sulu terrane, China. Chemical Geology, 2010, 269, 237-251.	3.3	84
220	Laser ablation ICP-MS titanite U–Th–Pb dating of hydrothermal ore deposits: A case study of the Tonglushan Cu–Fe–Au skarn deposit, SE Hubei Province, China. Chemical Geology, 2010, 270, 56-67.	3.3	160
221	Zircon U–Pb and trace element data from rocks of the Huai'an Complex: New insights into the late Paleoproterozoic collision between the Eastern and Western Blocks of the North China Craton. Precambrian Research, 2010, 178, 59-71.	2.7	112
222	Continental and Oceanic Crust Recycling-induced Melt-Peridotite Interactions in the Trans-North China Orogen: U-Pb Dating, Hf Isotopes and Trace Elements in Zircons from Mantle Xenoliths. Journal of Petrology, 2010, 51, 537-571.	2.8	2,939
223	NH4F assisted high pressure digestion of geological samples for multi-element analysis by ICP-MS. Journal of Analytical Atomic Spectrometry, 2010, 25, 408.	3.0	44
224	U-Pb age, trace-element, and Hf-isotope compositions of zircon in a quartz vein from eclogite in the western Dabie Mountains: Constraints on fluid flow during early exhumation of ultrahigh-pressure rocks. American Mineralogist, 2009, 94, 303-312.	1.9	78
225	Origin of a Mesozoic granite with A-type characteristics from the North China craton: highly fractionated from I-type magmas?. Contributions To Mineralogy and Petrology, 2009, 158, 113-130.	3.1	86
226	Delamination and destruction of the North China Craton. Science Bulletin, 2009, 54, 3367-3378.	9.0	126
227	Results for Rarely Determined Elements in MPIâ€DING, USCS and NIST SRM Glasses Using Laser Ablation ICPâ€MS. Geostandards and Geoanalytical Research, 2009, 33, 319-335.	3.1	32
228	Zircon U–Pb age, trace element and Hf isotope composition of Kongling terrane in the Yangtze Craton: refining the timing of Palaeoproterozoic highâ€grade metamorphism. Journal of Metamorphic Geology, 2009, 27, 461-477.	3.4	158
229	Age and nature of eclogites in the Huwan shear zone, and the multi-stage evolution of the Qinling-Dabie-Sulu orogen, central China. Earth and Planetary Science Letters, 2009, 277, 345-354.	4.4	146
230	Geochemical investigation of Early Cretaceous igneous rocks along an east–west traverse throughout the central Lhasa Terrane, Tibet. Chemical Geology, 2009, 268, 298-312.	3.3	367
231	牙å¼⁄¢çŸ³å¾®é‡å…ƒç´å⁻¹ç"Ÿç‰©ç»çë°‹ä»¶çš"å"尔:以二å•三åç³»å…∵ç∮å±,型剖é¢ç¬¬ä,€å¹•ç» Geosciences, 2009, 34, 725.	çë°dä»¶ä,° 0.5	ä¾ _Ó Diqiu Ke
232	Petrogenetic significance of high Fe/Mn ratios of the Cenozoic basalts from eastern China. Science in China Series D: Earth Sciences, 2008, 51, 229-239.	0.9	8
233	Direct Determination of Ag in Geological Samples by Membrane Desolvation-Inductively Coupled Plasma-Mass Spectrometer. Chinese Journal of Analytical Chemistry, 2008, 36, 1493-1498.	1.7	13
234	Niobium and Tantalum Concentrations in NIST SRM 610 Revisited. Geostandards and Geoanalytical Research, 2008, 32, 347-360.	3.1	20

#	Article	IF	CITATIONS
235	Geochronology and Hf isotopes of zircon from volcanic rocks of the Shuangqiaoshan Group, South China: Implications for the Neoproterozoic tectonic evolution of the eastern Jiangnan orogen. Gondwana Research, 2008, 14, 355-367.	6.0	263
236	Zircon U–Pb age and trace element evidence for Paleoproterozoic granulite-facies metamorphism and Archean crustal rocks in the Dabie Orogen. Lithos, 2008, 101, 308-322.	1.4	240
237	Accurate Determination of Rare Earth Elements in USGS, NIST SRM, and MPI-DING Glasses by Excimer LA-ICP-MS at High Spatial Resolution. Spectroscopy Letters, 2008, 41, 228-236.	1.0	24
238	Magnetic study of mafic granulite xenoliths from the Hannuoba basalt, north China. Geochemistry, Geophysics, Geosystems, 2008, 9, .	2.5	7
239	Petrogenesis and tectonic implications of Neoproterozoic, highly fractionated A-type granites from Mianning, South China. Precambrian Research, 2008, 165, 190-204.	2.7	108
240	Signal enhancement in laser ablation ICP-MS by addition of nitrogen in the central channel gas. Journal of Analytical Atomic Spectrometry, 2008, 23, 1093.	3.0	494
241	Recycling deep cratonic lithosphere and generation of intraplate magmatism in the North China Craton. Earth and Planetary Science Letters, 2008, 270, 41-53.	4.4	412
242	Recycled crust controls contrasting source compositions of Mesozoic and Cenozoic basalts in the North China Craton. Geochimica Et Cosmochimica Acta, 2008, 72, 2349-2376.	3.9	223
243	Fluids in deeply subducted continental crust: Petrology, mineral chemistry and fluid inclusion of UHP metamorphic veins from the Sulu orogen, eastern China. Geochimica Et Cosmochimica Acta, 2008, 72, 3200-3228.	3.9	145
244	Geochemistry and magmatic history of eclogites and ultramafic rocks from the Chinese continental scientific drill hole: Subduction and ultrahigh-pressure metamorphism of lower crustal cumulates. Chemical Geology, 2008, 247, 133-153.	3.3	504
245	Lithium isotopic composition and concentration of the deep continental crust. Chemical Geology, 2008, 255, 47-59.	3.3	98
246	In situ analysis of major and trace elements of anhydrous minerals by LA-ICP-MS without applying an internal standard. Chemical Geology, 2008, 257, 34-43.	3.3	3,342
247	A local aerosol extraction strategy for the determination of the aerosol composition in laser ablation inductively coupled plasma mass spectrometry. Journal of Analytical Atomic Spectrometry, 2008, 23, 1192.	3.0	111
248	è¶é«~压榴辉岩é‡ʻ红石ä,é«~场强åƒç′â∙åŒ−的控å^¶å›ç′åŠå¶åœ°çƒåŠ¨åŠ›å¦æ"빉. Diqiu Ko Geosciences, 2008, 33, 487.	exue - Zho 0.5	ngguo Dizhi I
249	Re–Os evidence for the age and origin of peridotites from the Dabie–Sulu ultrahigh pressure metamorphic belt, China. Chemical Geology, 2007, 236, 323-338.	3.3	49
250	Derivation of Mesozoic adakitic magmas from ancient lower crust in the North China craton. Geochimica Et Cosmochimica Acta, 2007, 71, 2591-2608.	3.9	163
251	Nd Isotopes and Geochemistry of Phanerozoic Clastic Sedimentary Rocks from the Yangtze Block and Their Tectonic Implications. Journal of China University of Geosciences, 2007, 18, 109-127.	0.5	2
252	Volume-optional and low-memory (VOLM) chamber for laser ablation-ICP-MS: application to fiber analyses. Journal of Analytical Atomic Spectrometry, 2007, 22, 582.	3.0	32

#	Article	IF	CITATIONS
253	A preliminary study of isopropyl alcohol matrix effect and correction in ICP-MS. Chinese Chemical Letters, 2007, 18, 1297-1300.	9.0	8
254	Timing of UHP metamorphism in the Hong'an area, western Dabie Mountains, China: evidence from zircon U–Pb age, trace element and Hf isotope composition. Contributions To Mineralogy and Petrology, 2007, 155, 123-133.	3.1	95
255	Trace elemental records of short-lived heating during exhumation of the CCSD eclogites. Science Bulletin, 2007, 52, 813-824.	1.7	20
256	Mesozoic crustal thickening of the eastern North China craton: Evidence from eclogite xenoliths and petrologic implications. Geology, 2006, 34, 721.	4.4	186
257	Mesozoic adakites in the Lingqiu Basin of the central North China Craton: Partial melting of underplated basaltic lower crust. Geochemical Journal, 2006, 40, 447-461.	1.0	15
258	Geochemistry and U-Pb zircon geochronology of Late-Mesozoic lavas from Xishan, Beijing. Science in China Series D: Earth Sciences, 2006, 49, 50-67.	0.9	25
259	Determination of Primary Magnetic Minerals of a Weathered Metapelite Xenolith from Zhouba Region, North China, by Combining Thermomagnetic Runs and Low-Temperature Measurements. Chinese Journal of Geophysics, 2005, 48, 946-952.	0.2	7
260	Nb/Ta variations of mafic volcanics on the Archean-Proterozoic boundary: Implications for the Nb/Ta imbalance. Science in China Series D: Earth Sciences, 2005, 48, 1106.	0.9	8
261	Suppression of interferences for direct determination of arsenic in geological samples by inductively coupled plasma mass spectrometry. Journal of Analytical Atomic Spectrometry, 2005, 20, 1263.	3.0	46
262	Melt–peridotite interactions: Links between garnet pyroxenite and high-Mg# signature of continental crust. Earth and Planetary Science Letters, 2005, 234, 39-57.	4.4	160
263	Zircon U-Pb ages of olivine pyroxenite xenolith from Hannuoba: Links between the 97?158 Ma basaltic under-plating and granulite-facies metamorphism. Science Bulletin, 2004, 49, 1055.	1.7	2
264	Recycling lower continental crust in the North China craton. Nature, 2004, 432, 892-897.	27.8	1,523
265	Petrology and geochemistry of spinel peridotite xenoliths from Hannuoba and Qixia, North China craton. Lithos, 2004, 77, 609-637.	1.4	505
266	Zircon U-Pb ages of olivine pyroxenite xenolith from Hannuoba: Links between the 97–158 Ma basaltic underplating and granulite-facies metamorphism. Science Bulletin, 2004, 49, 1055-1062.	1.7	6
267	Volatile organic solvent-induced signal enhancements in inductively coupled plasma-mass spectrometry: a case study of methanol and acetone. Spectrochimica Acta, Part B: Atomic Spectroscopy, 2004, 59, 1463-1470.	2.9	131
268	U–Pb zircon ages and Nd, Sr, and Pb isotopes of lower crustal xenoliths from North China Craton: insights on evolution of lower continental crust. Chemical Geology, 2004, 211, 87-109.	3.3	228
269	Thermodynamic evolution of lithosphere of the North China craton: Records from lower crust and upper mantle xenoliths from Hannuoba. Science Bulletin, 2003, 48, 2371.	1.7	20
270	Re–Os evidence for replacement of ancient mantle lithosphere beneath the North China craton. Earth and Planetary Science Letters, 2002, 198, 307-322.	4.4	802

Yong-Sheng Liu

#	Article	IF	CITATIONS
271	Geochemistry of lower crustal xenoliths from Neogene Hannuoba basalt, North China craton: implications for petrogenesis and lower crustal composition. Geochimica Et Cosmochimica Acta, 2001, 65, 2589-2604.	3.9	173
272	Magnetic structure of the continental crust as revealed by the Wutai-Jining crustal cross-section in the North China craton. Journal of Geodynamics, 2000, 29, 1-13.	1.6	10
273	Measured and calculated seismic velocities and densities for granulites from xenolith occurrences and adjacent exposed lower crustal sections: A comparative study from the North China craton. Journal of Geophysical Research, 2000, 105, 18965-18976.	3.3	48
274	Mechanism of Paleoarchean continental crust formation as archived in granitoids from northern part of Singhbhum Craton, eastern India. Geological Society Special Publication, 0, , SP489-2019-202.	1.3	7